Characterization of spatiotemporal chaos in arrays of nonlinear plasmonic nanoparticles

Zoheir Ziani, Gaëtan Lévêque,* and Abdellatif Akjouj
Université de Lille, Institut d'Electronique, de Micro-électronique et de Nanotechnologie (IEMN, UMR CNRS 8520), Département de Physique, 59652 Villeneuve d'Ascq, France

Saliya Coulibaly and Abdelmajid Taki
Université de Lille, CNRS, UMR 8523-PhLAM-Physique des Lasers Atomes et Molécules, F-59000 Lille, France

(Received 3 July 2019; revised manuscript received 4 October 2019; published 28 October 2019)

We investigate spatiotemporal chaos dynamics in a finite nanoparticles array with Kerr-type nonlinear response, excited by an incident plane wave of varying intensity and tunable frequency close to the localized plasmon resonance of a single particle. Considering dipole-dipole coupling between the nanoparticles described by their polarizability, we compute the temporal evolution of the dipoles and numerically extract the Lyapunov spectra, allowing us to characterize different dynamical behaviors. Furthermore, we estimate the Kaplan-Yorke dimension that provides a measure of the strange attractor complexity. We show that time-modulated solutions which are generated at the onset of modulational instability experience secondary instabilities leading to a complex nonlinear dynamic. It is also shown that in the highly nonlinear regime, the spatiotemporal chaos is robust and exists in a large range of parameters that we have determined numerically.

DOI: 10.1103/PhysRevB.100.165423

I. INTRODUCTION

Assemblies of metal nanoparticles (MNPs) allow manipulating light in compact photonic components by exploiting localized surface plasmon resonances (LSPs) [1]. Their ability to confine and enhance the intensity of light makes them choice elements for designing sensors [2], nanolasers [3], or interfaces for enhanced Raman spectroscopy [4] among other applications. In particular, chains of nanoparticles have been investigated for light waveguiding with subwavelength lateral confinement in experimental [5–7], analytical [8,9], and numerical [10,11] linear studies. Peculiar properties of LSPs allow increasing nonlinear processes close to resonance, and many theoretical and experimental investigations have been carried out within the plasmonics community concerning second-harmonic generation and two photon luminescence [12,13]. Other fascinating possibilities have been recently foreseen in exploiting third-order susceptibility of metal nanosystems, as they exhibit particular nonlinear plasmonics modes. The latter could be used for conceiving active photonic devices allowing to manipulate light in a new way: metal nanoantennas with Kerr-like susceptibility can show self-oscillation [14] and radiation switching [15], while one- or two-dimensional periodic assemblies of MNPs have recently been theoretically demonstrated to support bistability, switching waves [16], localized states like bright or dark solitons or oscillons [17–19], and Anderson localization [20]. However, little work has been performed on the extreme and fascinating case of spatiotemporal chaos.

Generally speaking, a chaotic dynamic reflects the persistence of an irregular behavior in a deterministic system with a small number of degrees of freedom. Hence, by extension, spatiotemporal chaos is the chaotic emergence of independent subdomains in a deterministic system with a large number of degrees of freedom. If its occurrence challenges the possibility of "controlling light with light" at the nanoscale, it can as well find applications in artificial intelligence [21–23] or communication encryption [24].

In this paper, we investigate spatiotemporal chaos (STC) in a linear chain of closely coupled silver nanoparticles (AgNPs) embedded in glass, under plane-wave excitation closely tuned to the LSP resonance of one single particle. Our findings show that our system only exhibits STC when subjected to an external homogeneous field with longitudinal polarization (electric field parallel to the chain axis), therefore we focus on this case in the following. We start with a brief reminder of the model and the dispersion relation method which allows us to analytically determine stationary homogeneous solutions and their stability [14,16,25,26]. Next, we present the theoretical procedure applied to characterize spatiotemporal chaos, based on the computation of Lyapunov spectra and the corresponding correlation length. We finally present our results, showing how our methodology allows a complete, quantitative characterization and robustness of the spatiotemporal chaos dynamics in a large range of parameters.

II. MODEL AND BASIC EQUATION

We consider the system of Fig. 1(a), consisting in a one-dimensional chain of identical spherical nanoparticles made of silver, that are embedded in a silica matrix with relative

*gaetan.leveque@univ-lille.fr

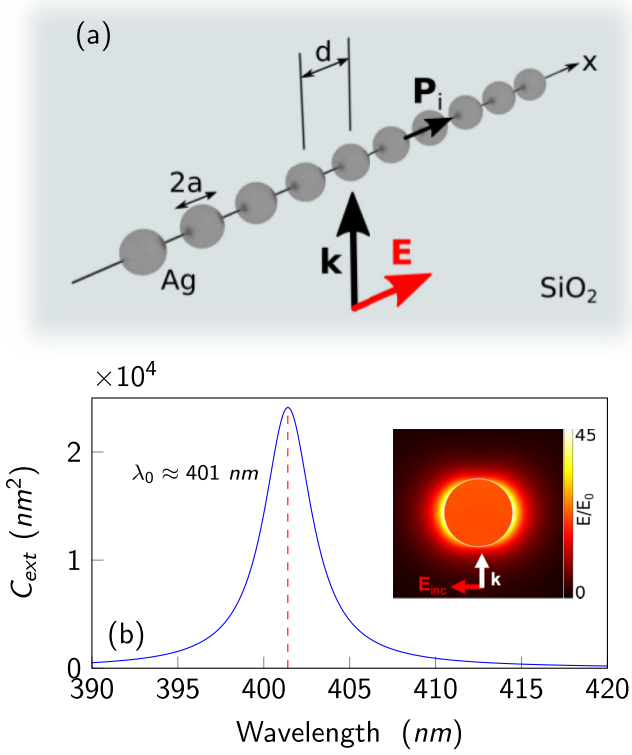

FIG. 1. (a) Schematic view of array of nanoparticles with a nonlinear response illuminated by an electric field with longitudinal polarization. (b) The extinction cross section C_{ext} as linear optical response of a spherical nanoparticle of silver with radius $a = 10$ nm. Insets show the amplitude of the electric near-field enhancement around the nanoparticle at the dipolar resonance $\lambda_0 \approx 401$ nm.

permittivity $\varepsilon_h \simeq 2.15$. The particle radius is $a = 10$ nm and the array period is $d = 30$ nm.

The linear response of a single AgNP shows a dipolar LSP resonance at $\lambda_0 \approx 401$ nm, with amplitude field enhancement reaching 20 inside the particle, Fig. 1(b). This large value induces enhanced nonlinear processes. We assume that the metal nanoparticles present a nonlinear Kerr-like response, and we define the nonlinear dielectric permittivity as

$$\varepsilon_{Ag}^{NL} = \varepsilon_\infty - \frac{\omega_p^2}{\omega(\omega - i\nu)} + \chi^{(3)}\left|\mathbf{E}_n^{(in)}\right|^2, \tag{1}$$

where $\varepsilon_\infty = 4.96$, $\hbar\omega_p = 9.54$ eV, $\hbar\nu = 0.055$ eV [27] [hereinafter we assume $\exp(i\omega t)$ time dependence], $\chi^{(3)} \simeq 3 \times 10^{-9}$ esu is the cubic susceptibility, and $\mathbf{E}_n^{(in)}$ is the local field inside the nth particle. Note that in centrosymmetric materials like silver or gold, the second-order nonlinearity is suppressed in volume and arises from symmetry breaking close to the metal interface, resulting in a small contribution compared to volume Kerr-like nonlinearity [28–30]. Finally, the chain is excited by an external plane wave with longitudinal polarization, with respect to the chain axis, and angular frequency ω close to the surface plasmon resonance ω_0 of an individual particle.

The array period d satisfies the condition $d \geqslant 3a$, and the wavelength of the driving field is much larger than a single sphere, so that we can consider spheres as point dipole [31] whose LSP angular frequency reads then $\omega_0 \approx \omega_p/\sqrt{\varepsilon_\infty + 2\varepsilon_h}$. According to Ref. [25], the temporal dynamical response of metal nanoparticle arrays excited by an arbitrary optical field fulfilling $\omega \approx \omega_0$ can be described by the following equation (explicit details are given in the Appendix):

$$-i\frac{dP_n}{d\tau} + (-i\gamma + \Omega + |P_n|^2)P_n + \sum_{m\neq n} G_{n,m}P_m = E_n, \tag{2}$$

where $P_n = p_n\sqrt{\chi^{(3)}}/(\sqrt{2(\varepsilon_\infty + 2\varepsilon_h)}\varepsilon_h a^3)$ and $E_n = -3\varepsilon_h\sqrt{\chi^{(3)}}E_n^{(ex)}/\sqrt{8(\varepsilon_\infty + 2\varepsilon_h)^3}$ are the dimensionless slowly varying amplitudes of respectively the longitudinal dipole moments and external electric fields, and $\gamma = \nu/2\omega_0 + (k_0 d)^3\varepsilon_h/(\varepsilon_\infty + 2\varepsilon_h)$ which describes thermal and radiation energy losses. The coefficient

$$G_{n,m} = \eta\left(\frac{ik_0 d}{|n-m|} + \frac{1}{|n-m|^2}\right)\frac{e^{-ik_0 d|n-m|}}{|n-m|}$$

is responsible for the dipole-dipole interaction between the nth and mth particles, $\tau = \omega_0 t$ is the dimensionless time, $\Omega = (\omega - \omega_0)/\omega_0$ is the detuning, $k_0 = \omega_0\sqrt{\varepsilon_h}/c$ is the wave number with c the speed of light, and the coupling coefficient is defined as $\eta = 3\varepsilon_h(a/d)^3/(\varepsilon_\infty + 2\varepsilon_h)$. The interaction is not limited to closest neighbors but involves all particles of the chain, even if the dependency on the distance makes it weaker for particles further away from each other [32]. This is an important difference between the above model corresponding to Eq. (2) and the discrete Lugiato-Lefever equation, where particles' interaction results from the discretized Laplacian term in the form $A(P_{n+1} + P_{n-1} - 2P_n)$, as investigated for instance in Ref. [33].

III. LINEAR STABILITY ANALYSIS

We focus our study on a plane wave normally incident onto the chain with longitudinal polarization, for which $E_n = E_0$ for all particles. Steady homogeneous solutions, corresponding to equal and constant dipole moments ($P_n = P_0$), can be obtained from Eq. (2) by setting $dP_n/d\tau = 0$, and are described by the following relation:

$$\left\{\left(|P_0|^2 + \Omega + \mathrm{Re}\sum_{j=1}^{+\infty}A_j\right)^2 + \left(\mathrm{Im}\sum_{j=1}^{+\infty}A_j - \gamma\right)^2\right\}|P_0|^2 = |E_0|^2, \tag{3}$$

where $A_j = 2\eta(j^{-3} + ik_0 dj^{-2})\exp(-ik_0 dj)$, and the symmetry $G_{n,m} = G_{m,n}$ has been taken into account in the summation. Any positive and real root $S_0 = |P_0|^2$ of Eq. (3) defines a steady homogeneous solution $P_0 = \sqrt{S_0}e^{i\varphi}$, where

$$\tan\varphi = \frac{\mathrm{Im}\,A_j - \gamma}{\Omega + Re\,A_j + S_0}. \tag{4}$$

Two examples of the dependence of $|P_0|^2$ on $|E_0|^2$ are shown in Fig. 2 corresponding to monostable and bistable regimes. Indeed, when $\Omega < \Omega_c = -\mathrm{Re}\sum_{j=1}^{+\infty}A_j - \sqrt{3}(\gamma - \mathrm{Im}\sum_{j=1}^{+\infty}A_j)$, $|P_0|^2$ becomes multivalued (red curve, bistable regime), while it is single valued for $\Omega > \Omega_c$ (blue curve, monostable regime). The transition between the two regimes

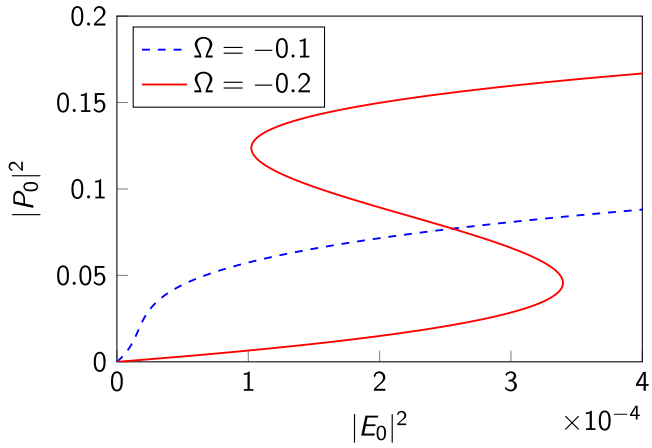

FIG. 2. Dependence of the absolute value of homogeneous polarization $|P_0|^2$ of the nanoparticles on the intensity of the external field $|E_0|^2$ for two cases depending on detuning parameter Ω: with $\Omega = -0.1$, the system is monostable, while when $\Omega = -0.2$, the system is bistable. The critical value is $\Omega_c = -0.1224$.

is illustrated by a movie in the Supplemental Material [34]. It has been recently shown that in the case of a transversal excitation [35], such a bistable dependence can support the existence of kinks and solitons [16].

Next, we study the linear stability of the homogeneous nonlinear state P_0 to a spatially harmonic perturbation in the form $\delta P_n = \delta P_0 \exp(-iKdn + \lambda\tau)$, where K is the modulation wave number, δP_0 is the amplitude of the perturbation ($|\delta P_0| \ll |P_0|$), and λ is the instability growth rate. Using the model Eq. (2) and expanding it to the first order in δP_0, we obtain the following dispersion relation [25]:

$$\lambda = \mathrm{Im}\sum_{j=1}^{+\infty} B_j - \gamma + \sqrt{|P_0|^4 - \left(2|P_0|^2 + \Omega + \mathrm{Re}\sum_{j=1}^{+\infty} B_j\right)^2}, \tag{5}$$

where we have set $B_j = A_j \cos(Kdj)$. The contour $\lambda = 0$ in the $(|P_0|^2, Kd)$ plane defines the neutral curve that determines the marginal stability where the steady state is neither amplified nor attenuated. It is given by the following equation:

$$|P_0|^2 = \frac{1}{3}\left\{-2\left(\Omega + \mathrm{Re}\sum_{j=1}^{+\infty} B_j\right) \pm \sqrt{\left(\Omega + \mathrm{Re}\sum_{j=1}^{+\infty} B_j\right)^2 - 3\left(\gamma - \mathrm{Im}\sum_{j=1}^{+\infty} B_j\right)^2}\right\}. \tag{6}$$

For any value of K for which λ is positive, the perturbation grows exponentially in time and the homogeneous solution P_0 is unstable. Figure 3 shows the instability domains in the plan $(|E_0|^2, |P_0|^2)$ and $(Kd, |P_0|^2)$, respectively, for a monostable regime. It appears that the growth rate λ reaches positive values in the excitation range $|E_0|^2 = 9 \times 10^{-6}$–$2.12 \times 10^{-3}$. At the bottom edge, the system destabilizes at the most unstable spatial frequency $Kd \approx 0.7$, whereas at the top edge, similar behavior occurs at $Kd = \pi$. Close to the two corresponding

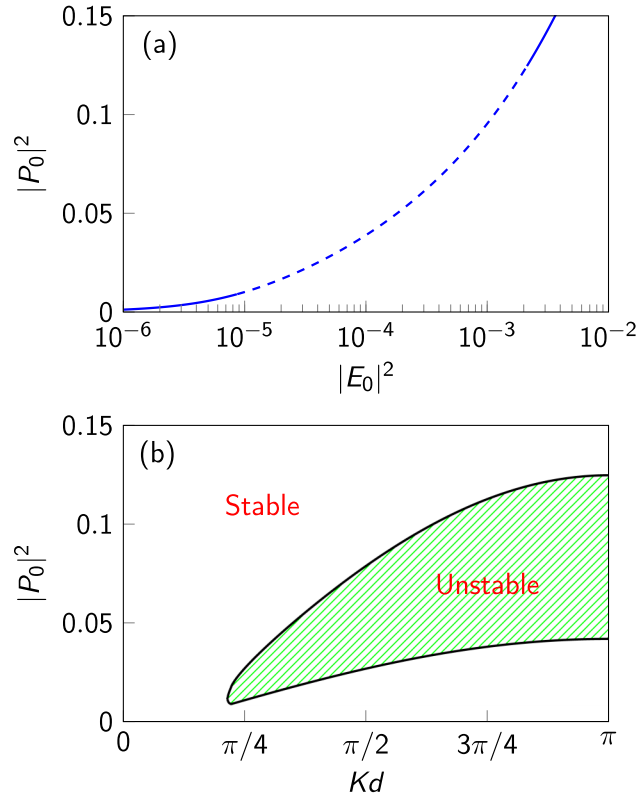

FIG. 3. (a) Homogeneous stationary solution $|P_0|^2$ as a function of the excitation intensity $|E_0|^2$. The solid line corresponds to stable states, the dashed line to unstable states. (b) Marginal stability curve, the system is unstable in the parameter domain within the curve. The detuning is set to $\Omega = -0.07$. Dotted horizontal lines show the limits of the instability.

pump values, the system presents stable harmonic spatial modulations, which evolve in more complex spatiotemporal dynamics for intermediate values. Inside the instability domain limited by the neutral curve [Fig. 3(b)], the nonlinear dynamics becomes more complex including transitions to spatiotemporal chaos. In the following, we focus on the occurrence and the characterization of spatiotemporal chaos, which appears in a large spectrum of wave numbers K.

IV. SPATIOTEMPORAL CHAOS

In the weak nonlinear limit, the statical description of the nonequilibrium behavior of random dispersive waves is well developed by the wave theory or order-parameter description, for dissipative systems [36]. Both approaches are known to provide the appropriate theoretical formulation. However, such approaches break down for strong nonlinearities, where the complex dynamic can be highly impacted by nonlinear excitations, e.g., solitons, collapses, and shocks. In this strong nonlinear regime, dominated by spatiotemporal chaos, no general theory exists. However, powerful mathematical tools have been developed to characterize spatiotemporal chaotic regimes. One popular tool is the generalized Lyapunov exponents (Lyapunov spectrum), which is particularly adapted to spatiotemporal systems [37,38]. Here, the characterization of complex dynamical behavior can be, indeed, achieved by

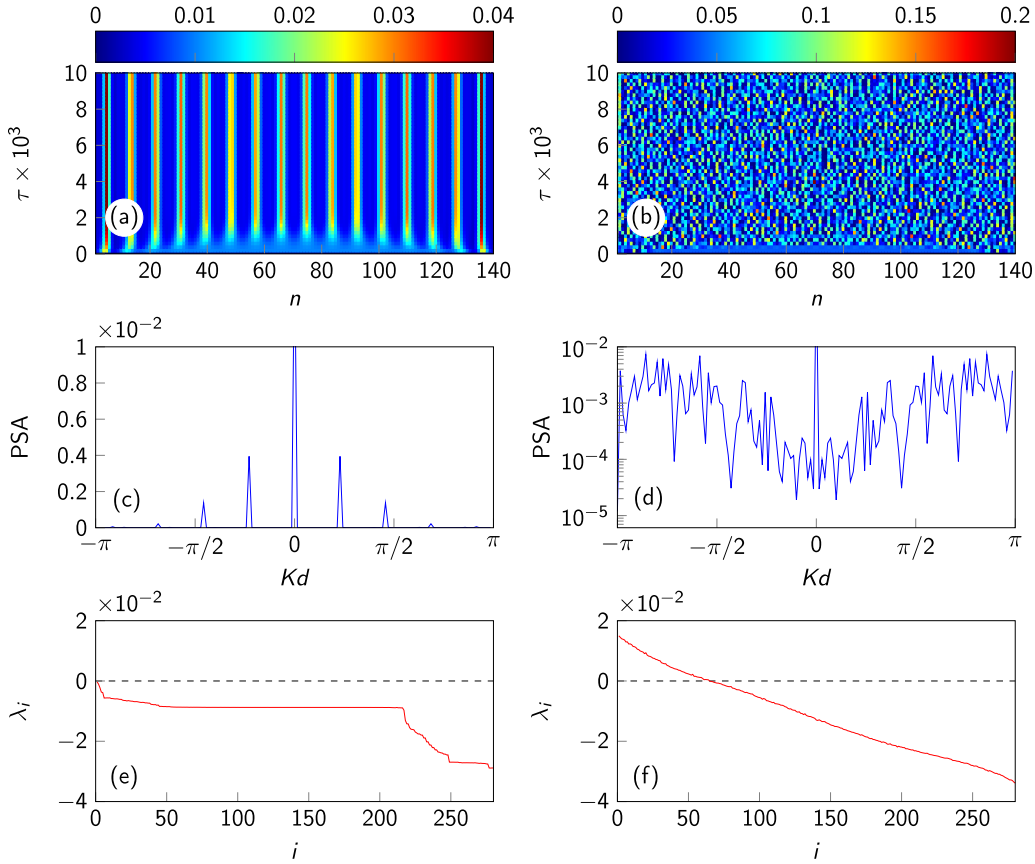

FIG. 4. For $\Omega = -0.07$, $N = 140$, and two pump intensities (left column: $|E_0|^2 = 1.00 \times 10^{-5}$; right column: $|E_0|^2 = 12.37 \times 10^{-5}$); (a) and (b) show the dynamic of $|P_n|^2$ obtained by numerical simulations of Eq. (2); (c) and (d) are the spatial spectra of the $|P_n|^2$ profile at $\tau = 10^4$; (e) and (f) are the spectra of Lyapunov exponents.

means of Lyapunov exponents, which provide information about permanent dynamics with sensitivity to close initial conditions [39]. When the largest Lyapunov exponent is positive, the system develops a chaotic regime but not necessarily a spatiotemporal chaos. To distinguish between these dynamical behaviors, it is necessary to determine the Lyapunov spectrum constituted by the set of exponents. Spatiotemporal chaos has a Lyapunov spectrum with a continuous set of positive values. In contrast, chaos possesses a Lyapunov spectrum with a discrete set of positive values. We have computed such exponents using a Gram-Schmidt orthonormalization process [40] on a finite chain of N nanoparticles. The Lyapunov exponents are labeled λ_i, where $i = 1, \ldots, 2N$. In our system, there are $2N$ Lyapunov exponents because each longitudinal dipole P_n is a complex scalar and possesses one degree of freedom (two dimensions). They are ordered such that $\lambda_p \leqslant \lambda_q$ $(p \geqslant q)$.

A typical situation is depicted in Fig. 4 where we show numerical results corresponding to a stable modulation ($\Omega = -0.07$ and $|E_0|^2 = 1 \times 10^{-5}$, left column) and a fully developed STC ($\Omega = -0.07$ and $|E_0|^2 = 12.37 \times 10^{-5}$, right column). The trajectories, calculated taking as an initial condition the homogeneous solution, are plotted in Figs. 4(a) and 4(b) together with the spatial Fourier transform of $|P_n|^2$ computed at $\tau = 10^4$ [Figs. 4(c) and 4(d)] and the Lyapunov spectra [Figs. 4(e) and 4(f)]. In the stable situation, the Fourier spectrum shows discrete harmonic frequencies, with a fundamental frequency $Kd \approx 0.7$, consistent with the value corresponding to the lowest edge of the instability area of Fig. 3. The associated Lyapunov spectrum has a complete set of negative values. In contrast, the STC regime is characterized by a continuous Fourier spectrum and a continuous set of positive values, confirming the spatiotemporal nature of the chaotic evolution.

From the spectra of Lyapunov exponents, we extract the Kaplan-Yorke dimension (D_{KY}), defined by [41]

$$D_{\mathrm{KY}} \equiv p + \frac{\sum_{i=1}^{p} \lambda_i}{|\lambda_{p+1}|} \tag{7}$$

where p is the largest integer satisfying $\sum_{i=1}^{p} \lambda_i > 0$. Figure 5 shows D_{KY} as a function of the number N of nanoparticles, and corresponding Lyapunov spectra. We see that this dimension increases linearly with the size of the system [42], which physically means that the structure and the complexity of the spatiotemporal chaos does not change with N, as long as it is large enough. Associated to the Kaplan-Yorke dimension, the slope of D_{KY} (see Fig. 5) as a function of N allows defining the quantity α through

$$\alpha = d\left(\frac{\partial D_{\mathrm{KY}}}{\partial N}\right)^{-1}. \tag{8}$$

This parameter constitutes an important characterization of the complexity of the spatiotemporal chaos; it is a function of

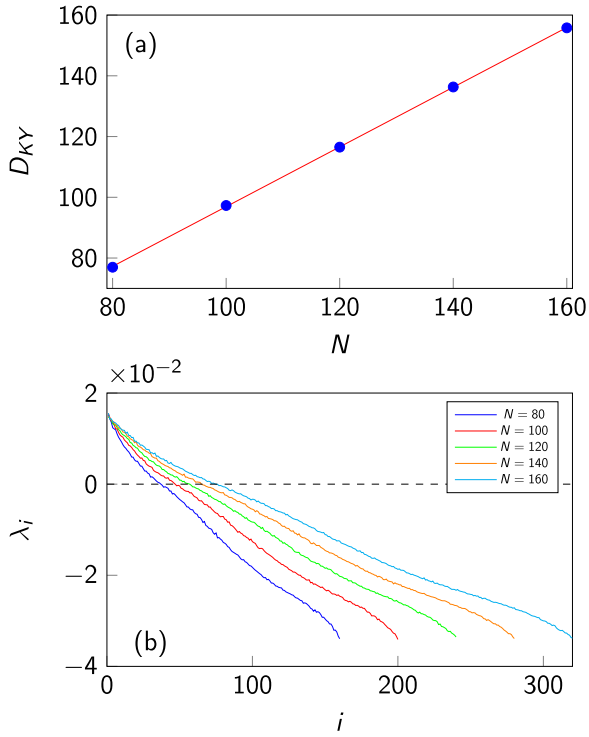

FIG. 5. (a) Kaplan-Yorke dimensions as a function of the number of particles N is indicated by the blue points for $\Omega = -0.07$ and $|E_0|^2 = 12.37 \times 10^{-5}$. The linear growth of D_{KY} dimension is fitted by a slope of 0.983, as shown by the red line. (b) The spectrum of Lyapunov exponents correspond to each number of particles N.

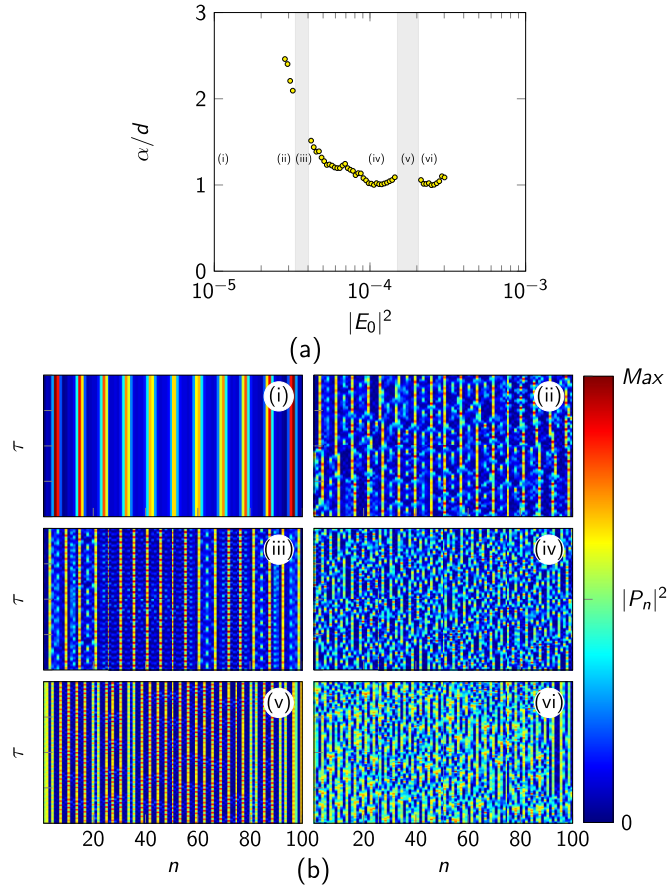

FIG. 6. (a) Lyapunov correlation length α as a function of the pump intensity $|E_0|^2$ for $\Omega = -0.07$; gray regions represent two windows of restabilization (auto-organized structures). (b) Illustrative trajectories for chosen values of the pump intensity: (i) 1×10^{-5}, (ii) 2.9×10^{-5}, (iii) 3.5×10^{-5}, (iv) 11×10^{-5}, (v) 18×10^{-5}, (vi) 22×10^{-5}.

the pump intensity $|E_0|^2$ and the detuning Ω, and is related to the correlation length of the chaotic subdomains within the system of nanoparticles. Its evolution is displayed on Fig. 6(a) as function of the excitation intensity for $\Omega = -0.07$. We notice that the correlation length reaches finite values only in a limited range of intensities in the middle of the instability domain. The correlation length decreases with the intensity until it reaches $\alpha/d \simeq 1$ in the vicinity of $|E_0|^2 = 10^{-4}$–3×10^{-4}, for which the system exhibits well developed STC and consecutive dipoles are almost uncorrelated. Finally, the correlation length quickly diverges and STC disappears, and a more ordered dynamic takes place. Moreover, in the two pump excitation windows, located at 1.5×10^{-4}–2×10^{-4} and 3×10^{-5}–4×10^{-5}, the system exhibits restabilization, where different localized structures such as oscillons [17] can be observed.

Typical trajectories have been plotted for chosen values of the pump intensities in the parameter domain where the correlation length reaches finite values. The aspect of those trajectories qualitatively agrees with the evolution of α with $|E_0|^2$. Restabilization is obvious in the first shaded window (iii), where trajectories are characterized by spatially quasistable oscillations, and in the second shaded window (v), where a more complex superposition of alternating stable dipoles, low amplitude large-scale front, and walking solitons is observed.

The strength of our method for characterizing STC chaos, through numerical computation of the Lyapunov correlation length, resides in its ability to completely quantify STC in the plane of control parameters $(\Omega, |E_0|^2)$, as shown in Fig. 7, where the inverse of the correlation length is plotted. To construct this figure, Lyapunov spectra have been computed for $N = 80, 100, \ldots, 160$ from trajectories. The Kaplan-Yorke dimension has been extracted from a linear regression of $D_{\mathrm{KY}}(N)$, and we only kept values for which the coefficient of determination is larger than 0.9. The STC domain is well bounded within the domain of modulational instability, and slightly overlap the bistability area, in blue. In this latter case, only the upper branch is unstable, so trajectories have been initialized with the corresponding stationary homogeneous solution. Few restabilization windows appear, around $(\Omega = -0.12,\ |E_0|^2 = 3 \times 10^{-4})$, $(\Omega = -0.07,\ |E_0|^2 = 2 \times 10^{-4})$, and $(\Omega = -0.07,\ |E_0|^2 = 3.5 \times 10^{-5})$. From Fig. 7, we can also deduce that the lower bound of the Lyapunov density dimension α is about $\alpha_{\min} = d/2$. As α is roughly interpreted as the range of the chaotic fluctuations, that is the minimal size chaotic subdomains, we can conclude that the intersphere distance d is an additional degree of freedom to control the spatiotemporal chaos in the system.

Finally, we can wonder if such a complex dynamical behavior is accessible to experimentation. As stated by Noskov

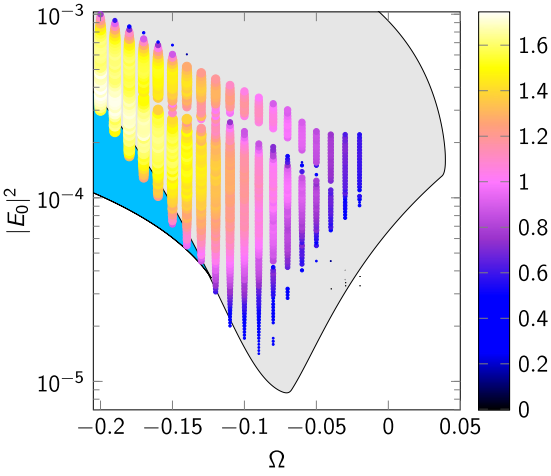

FIG. 7. Evolution of the inverse of the Lyapunov correlation length α/d, in the parameters plane $(\Omega, |E_0|^2)$. The gray background delimits the modulationally unstable domain for the monostable regime, while the blue one indicates the bistability domain, for which only the upper branch is unstable. The white background represents the stable domain for stationary homogeneous solutions.

et al. [16], large laser intensities can induce thermal damages to silver nanoparticles, but this effect could be avoided using picosecond pulses, long enough to observe STC as the transitory regime is about 10 fs while a characteristic time of the temporal chaos is about a few optical periods. Moreover, if measuring the time evolution of the dipoles of each nanoparticle can be difficult, chaos could be characterized probing the near field of a few particles within the chain, or directly working with the field scattered by the system, which can be used as an observable as it will contain a temporal signature of the STC.

V. CONCLUSION

In conclusion, we have investigated the complex spatiotemporal behavior of dipolar moments supported by spherical metal nanoparticles assembled in linear chains with subwavelength period. It has been shown that the onset of the spatiotemporal chaos when varying the pump power can be detected by computing Lyapunov spectra. When, for a fixed detuning, the pump power is increased from a stationary homogeneous solution, modulational instability arises first, characterized by only negative Lyapunov exponents. For larger pump powers, we observe a transition to continuous spectra with a subsequent set of positive exponents, characteristic of spatiotemporal chaos. We confirmed the nature of this behavior by verifying the linear increase of the Kaplan-Yorke dimension, extracted from the Lyapunov spectra, with the number of particles in the chain. From this extensive parameter, we were able to compute the Lyapunov density dimension, an intensive quantity corresponding to the characteristic size of the chaotic subdomains, which as such gives the measure of the spatiotemporal chaos as a function of the control parameters of the system. This powerful tool allows mapping the whole parameter space, which not only evidences the region of the spatiotemporal chaos inside the balloon delimiting the modulational instability, but also unveils stability islands within the chaotic region. Interesting openings can be foreseen, either exploiting the wide range of shapes and arrangements of nanoparticles made available by nanofabrication [43], or combining nonlinear plasmonics with emergent topics like topology [44]. Finally, we believe that this theoretical demonstration and characterization of the spatiotemporal chaos in an ensemble of subwavelength globally coupled plasmonic nanoparticles will be of interest for physical areas beyond plasmonic systems, since applications of spatiotemporal chaos spread all over the areas of modern nonlinear science.

APPENDIX: EQUATIONS FOR THE SLOWLY VARYING AMPLITUDES

We present a detailed landscape of the derivation of Eq. (2) which describes the nonlinear dynamics of the chain. We start from the Fourier transforms of the nth particle electric-dipole moments,

$$\alpha_n^{-1}(\omega)\mathbf{p}_n = \mathbf{E}_n^{(ex)} + \sum_{m\neq n} \mathbf{E}_{n,m}, \tag{A1}$$

where

$$\alpha_n(\omega) = \varepsilon_h \left\{ i\frac{2}{3}k^3 + \frac{\varepsilon_{Ag}^{NL}(\omega) + 2\varepsilon_h}{a^3\left[\varepsilon_{Ag}^{NL}(\omega) - \varepsilon_h\right]} \right\}^{-1} \tag{A2}$$

is the electric polarizability of the nth silver particle, and $\mathbf{E}_n^{(ex)}$ is the amplitude of the plane wave acting on the nth particle. The dipole-dipole interaction between mth and nth particle is given by

$$\mathbf{E}_{n,m} = \left((1 + ikd|n-m|)\frac{3(\mathbf{u}_0\cdot\mathbf{p}_m)\mathbf{u}_0 - \mathbf{p}_m}{\varepsilon_h |n-m|^3 d^3} + k^2 \frac{\mathbf{p}_m - (\mathbf{u}_0\cdot\mathbf{p}_m)\mathbf{u}_0}{\varepsilon_h |n-m| d} \right) e^{-ikd|n-m|}, \tag{A3}$$

where $\mathbf{u}_0$ is the unit vector going from the mth to the nth particle, and $k = (\omega/c)\sqrt{\varepsilon_h}$ is the wave number.

Since the frequency shift from the resonance value $\Delta\omega = \omega - \omega_0$ is too small, $|\Delta\omega|/\omega_0 \ll 1$, we decompose $\alpha_n^{-1}(\omega)$, which acts on the particle polarization, in the vicinity of $\omega_0 = \omega_p/\sqrt{\varepsilon_\infty + 2\varepsilon_h}$ to the first order of the Taylor series, and we take into account derivatives of time describing the widening of the light spectrum which is small,

$$\alpha_n^{-1}(\omega) \approx \alpha_n^{-1}(\omega_0) + \left.\frac{d\alpha_n^{-1}}{d\omega}\right|_{\omega=\omega_0} \left(\Delta\omega - i\frac{d}{dt}\right). \tag{A4}$$

Assuming that $\chi^{(3)}|\mathbf{E}_n^{(in)}|^2 \ll 1$ and $\nu/\omega_0 \ll 1$, we find that

$$\alpha_n^{-1}(\omega) \approx -\frac{1}{3a^3\varepsilon_h^2}\left[-i(\varepsilon_\infty + 2\varepsilon_h)\frac{\nu}{\omega_0} + \chi^{(3)}\left|\mathbf{E}_n^{(in)}\right|^2 - 2i(k_0 a)^3\varepsilon_h + \frac{2(\varepsilon_\infty + 2\varepsilon_h)}{\omega_0}\left(\Delta\omega - i\frac{d}{dt}\right)\right]. \tag{A5}$$

The local field inside the nth particle is given by

$$\begin{aligned}\mathbf{E}_n^{(in)} &= \frac{3\varepsilon_h}{\varepsilon_{Ag}+2\varepsilon_h}\left(\mathbf{E}_n^{(ex)}+\sum_{m\neq n}\mathbf{E}_{n,m}\right)\\ &= \frac{3\varepsilon_h}{\varepsilon_{Ag}+2\varepsilon_h}\alpha_n^{-1}(\omega)\mathbf{p}_n\\ &\approx \frac{3\mathbf{p}_n}{a^3[\varepsilon_{Ag}(\omega)-\varepsilon_h]}.\end{aligned} \tag{A6}$$

In the vicinity of the surface plasmon resonance of an individual particle ω_0, where we have $\varepsilon_{Ag}\approx -2\varepsilon_h$, we can write

$$\mathbf{E}_n^{(in)} \approx -\frac{\mathbf{p}_n}{\varepsilon_h a^3}. \tag{A7}$$

Replacing Eq. (A7) into Eq. (A5) and then into Eq. (A1), we have

$$\begin{aligned}&-i\frac{1}{\omega_0}\frac{d\mathbf{p}_n}{dt}+\left[\frac{\Delta\omega}{\omega_0}-i\left(\frac{\nu}{2\omega_0}+\frac{\varepsilon_h}{\varepsilon_\infty+2\varepsilon_h}(k_0a)^3\right)\right.\\ &\left.+\frac{\chi^{(3)}}{2\varepsilon_h^2a^6(\varepsilon_\infty+2\varepsilon_h)}|\mathbf{p}_n|^2\right]\mathbf{p}_n\\ &=-\frac{3a^3\varepsilon_h^2}{2(\varepsilon_\infty+2\varepsilon_h)}\left(\mathbf{E}_n^{(ex)}+\sum_{m\neq n}\mathbf{E}_{n,m}\right).\end{aligned} \tag{A8}$$

Introducing the dimensionless parameters $\tau=\omega_0 t$, $\Omega=\Delta\omega/\omega_0$, $\gamma=\nu/2\omega_0+(k_0a)^3\varepsilon_h/(\varepsilon_\infty+2\varepsilon_h)$, and

$$\mathbf{P}_n=\mathbf{p}_n\frac{\sqrt{\chi(3)}}{\sqrt{2(\varepsilon_\infty+2\varepsilon_h)\varepsilon_h a^3}}, \tag{A9}$$

$$\mathbf{E}_n=-3\varepsilon_h\mathbf{E}_n^{(ex)}\frac{\sqrt{\chi(3)}}{\sqrt{8(\varepsilon_\infty+2\varepsilon_h)^3}}, \tag{A10}$$

finally, we obtain the equation

$$-i\frac{d\mathbf{P_n}}{d\tau}+(-i\gamma+\Omega+|\mathbf{P_n}|^2)\mathbf{P_n}=\mathbf{E}_n-\sum_{m\neq n}\mathbf{A}_{n,m}, \tag{A11}$$

where

$$\begin{aligned}\mathbf{A}_{n,m}=\frac{\eta}{2}\Bigg((1+ikd|n-m|)\frac{3(\mathbf{u}_0\cdot\mathbf{P}_m)\mathbf{u}_0-\mathbf{P}_m}{|n-m|^3}\\ +(kd)^2\frac{\mathbf{P}_m-(\mathbf{u}_0\cdot\mathbf{P}_m)\mathbf{u}_0}{|n-m|}\Bigg)e^{-ikd|n-m|}\end{aligned} \tag{A12}$$

and

$$\eta=\frac{3\varepsilon_h}{(\varepsilon_\infty+\varepsilon_h)}\left(\frac{a}{d}\right)^3.$$

Taking into account that the relatively low strength of dipole-dipole interaction due to $\eta\propto(a/d)^3\ll 1$, we set $\mathbf{A}_{n,m}(k)=\mathbf{A}_{n,m}(k_0)$.

Considering a longitudinal excitation, in which $\mathbf{P}_m=\pm P_m\mathbf{u}_0$, we find

$$\mathbf{A}_{n,m}=\eta\left(\frac{ik_0d}{|n-m|}+\frac{1}{|n-m|^2}\right)\frac{e^{-ik_0d|n-m|}}{|n-m|}\mathbf{P}_m=G_{n,m}\mathbf{P_m}. \tag{A13}$$

[1] S. A. Maier, *Plasmonics: Fundamentals and Applications* (Springer Science & Business Media, New York, 2007).
[2] M. Li, S. K. Cushing, and N. Wu, Analyst **140**, 386 (2015).
[3] A. Yang, T. B. Hoang, M. Dridi, C. Deeb, M. H. Mikkelsen, G. C. Schatz, and T. W. Odom, Nat. Commun. **6**, 6939 (2015).
[4] B. Sharma, M. F. Cardinal, S. L. Kleinman, N. G. Greeneltch, R. R. Frontiera, M. G. Blaber, G. C. Schatz, and R. P. Van Duyne, MRS Bull. **38**, 615 (2013).
[5] J. R. Krenn, A. Dereux, J. C. Weeber, E. Bourillot, Y. Lacroute, J. P. Goudonnet, G. Schider, W. Gotschy, A. Leitner, F. R. Aussenegg *et al.*, Phys. Rev. Lett. **82**, 2590 (1999).
[6] S. A. Maier, M. L. Brongersma, P. G. Kik, and H. A. Atwater, Phys. Rev. B **65**, 193408 (2002).
[7] A. F. Koenderink, R. de Waele, J. C. Prangsma, and A. Polman, Phys. Rev. B **76**, 201403 (2007).
[8] M. L. Brongersma, J. W. Hartman, and H. A. Atwater, Phys. Rev. B **62**, R16356 (2000).
[9] L. Dobrzynski, A. Akjouj, B. Djafari-Rouhani, J.-O. Vasseur, M. Bouazaoui, J.-P. Vilcot, H. Al Wahsh, P. Zielinski, and J. P. Vigneron, Phys. Rev. E **69**, 035601(R) (2004).
[10] I. L. Rasskazov, S. V. Karpov, and V. A. Markel, Phys. Rev. B **90**, 075405 (2014).
[11] I. L. Rasskazov, S. V. Karpov, G. Y. Panasyuk, and V. A. Markel, J. Appl. Phys. **119**, 043101 (2016).
[12] M. Kauranen and A. V. Zayats, Nat. Photon. **6**, 737 (2012).
[13] J. Wang, J. Butet, A.-L. Baudrion, A. Horrer, G. Lévêque, O. J. Martin, A. J. Meixner, M. Fleischer, P.-M. Adam, A. Horneber *et al.*, J. Phys. Chem. C **120**, 17699 (2016).
[14] N. Lapshina, R. Noskov, and Y. S. Kivshar, JETP Lett. **96**, 759 (2013).
[15] R. Noskov, A. Krasnok, and Y. S. Kivshar, New J. Phys. **14**, 093005 (2012).
[16] R. E. Noskov, P. A. Belov, and Y. S. Kivshar, Opt. Express **20**, 2733 (2012).
[17] R. Noskov, P. Belov, and Y. Kivshar, Sci. Rep. **2**, 873 (2012).
[18] R. E. Noskov, D. A. Smirnova, and Y. S. Kivshar, Philos. Trans. R. Soc., A **372**, 20140010 (2014).
[19] R. E. Noskov, D. A. Smirnova, and Y. S. Kivshar, Opt. Lett. **38**, 2554 (2013).
[20] Z. Mai, F. Lin, W. Pang, H. Xu, S. Tan, S. Fu, and Y. Li, Opt. Exp. **24**, 13210 (2016).
[21] M. Naruse, Y. Terashima, A. Uchida, and S.-J. Kim, Sci. Rep. **7**, 8772 (2017).
[22] M. Naruse, T. Mihana, H. Hori, H. Saigo, K. Okamura, M. Hasegawa, and A. Uchida, Sci. Rep. **8**, 10890 (2018).
[23] S. Kumar, J. P. Strachan, and R. S. Williams, Nature (London) **548**, 318 (2017).
[24] S. Banerjee, L. Rondoni, S. Mukhopadhyay, and A. P. Misra, Opt. Commun. **284**, 2278 (2011).

[25] R. E. Noskov, P. A. Belov, and Y. S. Kivshar, Phys. Rev. Lett. **108**, 093901 (2012).
[26] R. E. Noskov, A. A. Zharov, and M. V. Tsarev, Phys. Rev. B **82**, 073404 (2010).
[27] S. Kawata and P. Verma, in *Metamaterials: Fundamentals and Applications II*, edited by M. A. Noginov, N. I. Zheludev, A. D. Boardman, and N. Engheta, Proceedings of SPIE, Vol. 7392 (SPIE, Bellingham, WA, 2009).
[28] M. Danckwerts and L. Novotny, Phys. Rev. Lett. **98**, 026104 (2007).
[29] G. Sartorello, N. Olivier, J. Zhang, W. Yue, D. J. Gosztola, G. P. Wiederrecht, G. Wurtz, and A. V. Zayats, ACS Photon. **3**, 1517 (2016).
[30] B. K. Canfield, H. Husu, J. Laukkanen, B. Bai, M. Kuittinen, J. Turunen, and M. Kauranen, Nano Lett. **7**, 1251 (2007).
[31] S. Y. Park and D. Stroud, Phys. Rev. B **69**, 125418 (2004).
[32] C. A. Downing, E. Mariani, and G. Weick, J. Phys.: Condens. Matter **30**, 025301 (2018).
[33] M. Clerc, S. Coulibaly, M. Ferré, and R. Rojas, Chaos **28**, 083126 (2018).
[34] See Supplemental Material at http://link.aps.org/supplemental/10.1103/PhysRevB.100.165423 for animation showing side-by-side, the relation with frequency between the stationary homogeneous solutions $|P_0|^2$ and the external field intensity $|E_0|^2$ (the dashed line corresponds to unstable solutions), and the related cut in the parameter plane $(\Omega, |E_0|^2)$.
[35] W. H. Weber and G. W. Ford, Phys. Rev. B **70**, 125429 (2004).
[36] H. Urra, J. F. Marín, M. Páez-Silva, M. Taki, S. Coulibaly, L. Gordillo, and M. A. García-Ñustes, Phys. Rev. E **99**, 033115 (2019).
[37] S. Nazarenko, *Wave Turbulence* (Springer Science & Business Media, New York, 2011), Vol. 825.
[38] Z. Liu, M. Ouali, S. Coulibaly, M. Clerc, M. Taki, and M. Tlidi, Opt. Lett. **42**, 1063 (2017).
[39] A. Pikovsky and A. Politi, *Lyapunov Exponents: A Tool to Explore Complex Dynamics* (Cambridge University Press, Cambridge, UK, 2016).
[40] A. Wolf, J. B. Swift, H. L. Swinney, and J. A. Vastano, Phys. D (Amsterdam, Neth.) **16**, 285 (1985).
[41] P. Frederickson, J. L. Kaplan, E. D. Yorke, and J. A. Yorke, J. Differential Equations **49**, 185 (1983).
[42] D. Ruelle, Commun. Math. Phys. **87**, 287 (1982).
[43] D. Eschimese, F. Vaurette, D. Troadec, G. Leveque, T. Melin, and S. Arscott, Sci. Rep. **9**, 7682 (2019).
[44] C. A. Downing and G. Weick, Eur. Phys. J. B **91**, 253 (2018).